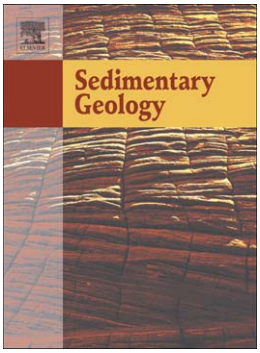

Mid-Eocene alluvial-lacustrine succession at Gebel El-Goza El-Hamra (NE Eastern Desert, Egypt): Facies analysis, sequence stratigraphy and paleoclimatic implications

H.A. Wanas, E. Sallam, M.K. Zobaa, X. Li

PII: S0037-0738(15)00199-2
DOI: doi: 10.1016/j.sedgeo.2015.09.006
Reference: SEDGEO 4907

To appear in: *Sedimentary Geology*

Received date: 14 August 2015
Revised date: 17 September 2015
Accepted date: 18 September 2015

Please cite this article as: Wanas, H.A., Sallam, E., Zobaa, M.K., Li, X., Mid-Eocene alluvial-lacustrine succession at Gebel El-Goza El-Hamra (NE Eastern Desert, Egypt): Facies analysis, sequence stratigraphy and paleoclimatic implications, *Sedimentary Geology* (2015), doi: 10.1016/j.sedgeo.2015.09.006

Mid-Eocene alluvial-lacustrine succession at Gebel El-Goza El-Hamra (NE Eastern Desert, Egypt): Facies analysis, sequence stratigraphy and paleoclimatic implications

H. A. Wanas[1,*], E. Sallam[2], M. K. Zobaa[2,3], X. Li[4]

[1] Geology Department, Faculty of Science, Menoufiya University, Shebin El-Kom, Egypt

[2] Geology Department, Faculty of Science, Benha University, Benha 13518, Egypt

[3] Department of Geosciences and Geological and Petroleum Engineering, Missouri University of Science and Technology, USA

[4] School of Earth Sciences and Engineering, Nanjing University, Nanjing, China

*** Corresponding author**: hamdallawanas@yahoo.com (H.A. Wanas)

E-mails: emad.salam@fsc.bu.edu.eg (E. Sallam); mohamed.zobaa@fsc.bu.edu.eg (M.K. Zobaa); leeschhui@126.com (Xianghui Li)

Keywords: Alluvial floodplain**;** lacustrine; Sequence stratigraphy; Paleopedogenesis; Paleoclimate; Bartonian; Egypt

ABSTRACT

This study aims to provide the depositional facies, sequence stratigraphic and paleoclimatic characteristics of the Mid-Eocene (Bartonian) continental succession exposed at Gebel El-Goza El-Hamra (Shabrawet area, NE Eastern Desert, Egypt). The studied succession consists of siliciclastic rocks followed upward by carbonate rocks. Detailed field observation and petrographic investigation indicate accumulation in floodplain-dominated alluvial and shallow lacustrine systems. The floodplain-dominated alluvial facies (45 m thick) is composed mainly of carbonate nodules-bearing, mottled mudrock with subordinate sandstone and conglomerate beds. The conglomerate and pebbly sandstone bodies interpreted as ephemeral braided channel deposits. The massive, laminated, planner cross-bedded, fine- to medium-grained sandstone bodies interlayered within mudstone reflect sheet flood deposits. The mudstones associated with paleosols represent distal floodplain deposits. The shallow lacustrine facies (15 m thick) is made up of an alternation of marlstone, dolostone and mudrock beds with *charophytes* and small gastropods. Pollen assemblages, stable $\delta^{18}O$ and $\delta^{13}C$ isotopes, and paleopedogenic features reflect prevalence of arid to semi-arid climatic conditions during the Bartonian.

The sequence stratigraphic framework shows an overall fining-upward depositional sequence, consisting of Low- and High-accommodation Systems Tracts (LAST, HAST), and is bounded by two sequence boundaries (SB-1, SB-2). Conglomerate and pebbly sandstone deposits (braided channel and sheet flood deposits) of the lower part of the alluvial facies (FA-1) reflect a

LAST. Mudrock and silty claystone facies (distal floodplain deposits) of the upper part of alluvial floodplain facies (FA-1) and its overlying lacustrine facies (FA-2) correspond to a HAST. The LAST, HAST and SB were formed during different accommodation-to-sediment supply (A/S) ratio phases. The variation in A/S ratios was mainly controlled by sea-level change as well as by local tectonic subsidence and uplift of the basin coincident with the reactivation of the Syrian Arc System during the Bartonian.

1. Introduction

Interest in alluvial-lacustrine deposits has increased worldwide because significant clues to the climatic, tectonic and environmental conditions on local, regional and global scales (e.g., Gierlowski-Kordesch, 1998; Abdul Aziz et al., 2003; Huerta and Armenteros, 2005; Alonso-Zarza et al., 2009; Gurel and Kadir, 2010; Alçiçek and Jiménez-Moreno, 2013). Sequence stratigraphy of alluvial-lacustrine successions has been analyzed in detail (e.g., Shanley and McCabe, 1994; Martinsen et al., 1999; Plint et al., 2001; Cleveland et al., 2007; Fanti and Catuneanu, 2010; Scherer et al., 2015), but still there is discussion about the sequence stratigraphic elements in this kind of sedimentary successions. The alluvial-lacustrine successions of the Mid-Eocene (Bartonian) of Egypt have never been studied in detail to ascertain their depositional environments, sequence stratigraphy and paleoclimatic conditions.

Previous geologic studies of the Mid-Eocene rocks in the area under investigation focused on their stratigraphy (Al-Ahwani, 1982; Shamah and Helal, 1993; Abu El-Ghar, 2007; Selim et al., 2012; Sallam et al., 2015). Recently, Selim et al. (2012) and Sallam et al. (2015) reported the occurrence of continental deposits in the Mid-Eocene (Bartonian) rocks. No previous work exists on the sedimentological, sequence stratigraphic and paleoenvironmental characteristics of these Bartonian continental deposits. The present study aims to address the depositional facies, sequence stratigraphy and paleoclimatic characteristics of this continental succession. This will be achieved through integrated field, petrographic, geochemical (stable $\delta^{18}O$, $\delta^{13}C$ isotopes) and pollen analyses of the Bartonian rocks.

2. Geological setting and lithostratigraphy

The Shabrawet area lies on the western side of the Great Bitter Lakes close to the Suez Canal in the Eastern Desert of Egypt (Fig. 1). The Shabrawet area is situated in the unstable tectonic shelf area of the African cratonic margin (Said, 1990). It represents a segment of the Syrian Arc System developed in the southern margin of Tethys on a NE–SW trend (Said, 1990). The Syrian Arc System was renewed and enlarged several times during the late Cretaceous up to the Neogene (Said, 1990). It includes a number of asymmetrical anticlines and synclines stretching from Libya to the west via north Egypt and further northeast into Levant. Two ENE-oriented asymmetrical plunging anticlines, enclosing a shallow syncline, were recognized in the Shabrawet area, and named as Gebel Shabrawet East and

Gebel Shabrawet West (Al-Ahwani, 1982). The Cretaceous rocks form the cores of these anticlines and are unconformably overlain by nearly horizontal Eocene, Oligocene and Miocene strata (Al-Ahwani, 1982; Haggag, 2010). The Shabrawet area was also influenced by a major NW–SE fault that resulted in the displacement of the Eocene and younger rocks against the older Cretaceous strata (Haggag, 2010).

Lithostratigraphically, the oldest exposed rock unit in the Gebel Shabrawet area is the Malha Formation (Aptian–Albian) that crops out at the core of Gebel Shabrawet East anticline (Haggag, 2010). The Malha Formation is followed upwards by the Galala Formation (Cenomanian), the Maghra El-Hadida Formation (Turonian–Santonian) and the Maghra El-Bahari Formation (late Cretaceous–early Paleogene), respectively (Al-Ahwani, 1982; Haggag, 2010) (Fig. 1). These formations are unconformably overlain by a thick Eocene succession that is in turn disconformably overlain by Oligocene rocks (Fig. 1). The Eocene succession has been subdivided into three lithostratigraphic units (Sallam et al. 2015) that are from base to top: the Minia Formation (late Ypresian), the Sannor Formation (Bartonian) and the Maadi Formation (Priabonian) (Fig. 1). At Gebel El-Goza El-Hamra, the Bartonian Sannor Formation was lithologically subdivided into three informal units: lower (Sn-1), middle (Sn-2), and upper (Sn-3) (Sallam et al., 2015, Fig. 2).

In the study area, the Mid-Eocene (Bartonian) rocks represent the middle unit (Sn-2) of the Sannor Formation of Sallam et al. (2015). They form

a succession consists mainly of siliciclastic rocks topped by carbonate beds that overall reach up a maximum thickness of 60 m (Figs. 2, 3). They crop out in gently sloped small hills separated by small incised water gullies (Fig. 4a). These rocks are barren in marine fossils and are clearly distinguishable from the underlying and overlying foraminiferal limestones (Fig. 4b). The strata display wedge-shaped geometry in cross section, and pinching out laterally to the south and southwest. Lithologically, the studied succession can be subdivided into lower, middle, and upper parts (Fig. 4b, c). The lower part (20 m thick) consists mainly of yellow mudrock and clayey siltstone intercalated with some beds (0.5–1.0 m thick) of pebbly sandstone and conglomerate (Fig. 4d). The middle part (25 m thick) is made up of white silty mudrock showing purple, violet to bloody red colour mottling (Fig. 4e). The upper part (15 m thick) is composed of alternating beds of yellow dolostone, grayish yellow marlstone and reddish grey mudrock (Figs. 2, 3).

3. Methods and analytical techniques

High-resolution sedimentary logs were described and measured in outcrops to define the main facies and facies associations. Facies were classified following Miall's (1978) code system. The facies were grouped in facies associations which, according to Miall (2010) correspond to genetically-related sub-environments within a depositional system. The sequence stratigraphic elements (stratigraphic key surfaces and systems tracts) were mapped through facies architecture and stacking pattern of the studied strata. Twenty eight thin-sections from collected samples were prepared and

investigated using standard polarizing microscopy to define micro-textural features. Five samples (EGH-6, 7, 8, 9, 11) were selected from the mudrocks intervals for pollen analysis. For this analysis, the samples were prepared following the conventional palynological maceration techniques as described in Zobaa et al. (2013). The prepared kerogen slides were scanned and counted using transmitted light microscopy under variable magnifications to qualitatively and quantitatively document their total particulate organic matter (POM) content. Pollen grains were photographed using an Olympus BX51 light microscope equipped with an integrated Olympus LC20 digital camera.

Small fresh chips of some samples were prepared by gold-coating and investigated under Scanning Electron Microscope (SEM) equipped with an energy-dispersive analyzer (EDX). The SEM was performed to illustrate the grain, matrix and cement morphologies in the samples. The EDX was used to semi-quantitative estimates of rock-forming minerals. The mineralogical analysis was carried out on non-oriented (bulk mineralogy) samples by using X-ray diffraction (XRD) technique. XRD analyses were performed using a Philips PW1752 diffractometer with Ni filter and Cu-Kα radiation (λ= 1.54060 Å) operating at 40kv and 30 mA, a step size of 2θ is 0.02º and time per step of 2 s. The XRD was used to just confirm the petrographic mineralogical observations. Carbon and oxygen isotopic values were determined for 11 carbonate samples. For oxygen and carbon isotopic analyses, small amounts of carbonate powder were micro-drilled from each sample and homogenized. Powders of 0.5–1.0 mg were then dried and placed

in an oven at 70 °C for 10 hours before being moved to the instrument. Carbon dioxide was released using orthophosphoric acid at 70 °C and analyzed on-line in a DELTA plus XP + Gas Bench mass spectrometer. The precision of measurements was regularly checked with the Chinese national carbonate standard (GBW04405) and the international standard (NBS19). The standard deviation of $\delta^{13}C$ was ±0.1‰ over the period of analysis. Calibration to the international Pee Dee Belemnite (PDB) scale was performed using NBS19 and NBS18 standards. XRD was analyzed at the Center of Modern Analysis, Nanjing University, P.R. China. Measurements of SEM-EDX and carbon isotope were made at State Key Laboratory of Mineral Deposit Research, Nanjing University, P.R. China. Mottle colours were identified based on Munsell's rock color charts (2001).

4. Depositional facies and related environments

Two distinct facies associations (FA) that are characteristic for two main depositional environments were recognized (Figs. 2, 3, Table 1): floodplain-dominated alluvial facies association (FA-1), and shallow lacustrine/palustrine facies association (FA-2).

4.1. Floodplain-dominated alluvial facies association: FA-1

FA-1 is characterized by clayey siltstone and silty claystone with subordinate sandstone and conglomerate bodies. The strata of FA-1 attain 45 m thick, and occupy the basal two-thirds of the studied succession (Figs. 2, 3). This floodplain-dominated alluvial facies association (FA-1) includes three

lithofacies types: clast- and matrix-supported conglomerate (*Gcm; Gmm* and *Gh*), massive, laminated to planar cross-bedded sandstone (*Sm, Sh* and *Sp*), and mottled massive claystone–clayey siltstone-mudrock (*Fsm and Fm*) (Table 1). These three lithofacies types were interpreted to be deposited in three alluvial sub-environments: ephemeral braided channel, sheet flood and distal floodplain, respectively (Table 1).

4.1.1.Clast- and matrix-supported conglomerate lithofacies: Gcm, Gmm and Gh

*Description***:** This lithofacies is mainly represented by conglomerate beds. It occurs in the lower part of the studied rock unit (Figs. 2, 3). The conglomerate deposits form few interbeds within the mudrock (claystone and clayey siltstone) (Fig. 4d). The conglomerate beds display large-scale lensoidal bed geometry (Fig. 5a), although several laterally persistent sheet-like bodies are locally present (Fig. 5b). The conglomerate beds display basal erosional (scoured) surfaces with the underlying desiccated mudrock (Fig. 5c). Thickness of the individual conglomerate bodies varies between 0.3 and 1.5 m. The conglomerate is brownish grey in colour, showing both matrix- and clast-supported fabrics. The clast-supported conglomerate (*Gcm*) is characterized by pebble- to cobble-grade, poorly-sorted, rounded to well-rounded, elongated and discoidal clasts, that are formed mainly of dolomite, limestone, flint, quartz and other dark-colored rock fragments (Fig. 5c). These conglomerate deposits display massive disorganized clast fabric, with occasionally clast imbrication (*Gh*) (Fig. 5d). The matrix-supported

conglomerate *(Gmm*) is characterized by poorly-sorted, sub-rounded pebbles and cobbles. The pebbles and cobbles are composed of dolomite, limestone, quartz and flint embedded in argillaceous groundmass. They also show inverse grading and non-erosional bases (Fig. 5d).

Interpretation: Matrix- and clast-supported conglomerate deposits are mostly attributed to alluvial coarse deposits flowing from adjacent uplifted ional hinterland areas (e.g., Miall, 1996, 2010). The clast-supported, lenticular, poorly-sorted, polymictic conglomerate can be interpreted as in-channel elongated-shaped gravel bars deposited from ephemeral braided stream reaches of an alluvial plain, with erratic flow and high discharge rate (Miall, 1978). The local occurrence of clast imbrication suggests lag deposits formed by traction deposition via rolling and dragging along (Miall, 1978, 2010). Clast imbrication displays a unidirectional paleocurrent pattern towards the south and southwest, reflecting deposition under the influence of a powerful current (Selley, 1996; Miall, 2010). The presence of erosional bases indicates turbulent flow (Selley, 1996). The poorly-sorted matrix-supported conglomerate *(Gmm*) in between mudrocks can be interpreted as gravity driven plastic debris-flow deposits with concurrent transport of a mixture sediment load of mud, sand and gravel (Nemec and Steel, 1984). They also suggest intermittent flash floods or hyper-concentrated flows with high discharge rates (Miall, 2010, and references therein).

4.1.2. Massive, laminated and planar cross-bedded sandstone lithofacies: Sm, Sh and Sp

-Description: This lithofacies occurs in the basal part of the studied rock unit. It comprises few sandstone beds within the dominant yellow-colored mudrock (claystone and clayey siltstone) (Figs. 2, 3). The sandstone is fine- to medium-grained, pebbly and moderately-sorted. Most of the sandstone beds show sheet-like geometry and massive internal structure (*Sm*) (Fig. 5c), while some of them exhibit horizontal lamination (*Sh*) and occasional small-scale planar cross-bedding (*Sp)* (Fig. 5e). The observed planar cross-bedding pointed to unidirectional paleocurrent, generally towards the west and northwest. The sandstone deposits are faint yellow in colour and contain randomly distributed pebbles with matrix of silty- and clayey-sized particles. Thickness of individual sandstone bodies varies from 0.5 m to 1.5 m. The sandstone beds show sharp erosional bases and are truncated by a sandy conglomerate unit at top.

Interpretation: The occasional occurrence of unidirectional planar cross-bedded sandstone beds within the mudrock is attributed to downstream migration of transverse bars and sand waves in shallow water stream channels under upper flow regime conditions (Miall, 1996, 2010). The intercalated sheet-like geometry thin beds of pebbly fine-to medium-grained sandstone within mudrock probably represent episodic sheet-floods discharged into the distal alluvial-floodplain (Kraus and Gwinn, 1997; Abdul Aziz et al., 2003; Alçiçek and Jiménez-Moreno, 2013). Similar sheet-flood deposits have been interpreted as a sandy accumulation in wide alluvial-plains during unconfined overbank flooding of major fluvial systems under upper flow regime (Kraus

and Gwinn, 1997; Fisher et al., 2007), in many cases corresponding to short-lived braided rivers (Selley, 1996; Miall, 2010).

4.1.3. Massive claystone–clayey siltstone and mudrock lithofacies: Fsm and Fm

Description: This lithofacies is the most abundant in the lower and middle parts of the studied rock unit (Figs. 2, 3). The lower and upper boundaries of *Fsm* and *Fm* are erosional and sharp (Fig. 5b, c). In the lower part (2-2.5 m thick) of the studied succession, the mudrock deposits are faint yellow including reddish white mottles in the form of downward stripes (Fig. 5e, f). In this part, the claystone and clayey siltstone beds include some conglomerate and fine-grained sandstone interbeds (Fig. 4d). Some mudrock beds enclose scattered, sub-rounded carbonate nodules (4-7 cm in diameter; Fig. 5g) and dispersed black carbonaceous? (organic) matter (Fig. 5h). The mudrock deposits in the middle part (9–12 m thick) of the studied succession are white and show red to purple mottles occurring as vertically-oriented, downward stripes (Figs. 4e, 6a). They also display colour mottles in the form of dispersed patches and irregular forms (Fig. 6b). Low-angle cracks filled by reddish white clays are also noted in mudrock (Fig. 6c).

Interpretation: The claystone, clayey siltstone and mudrock are barren of marine fossils, and are interpreted as characteristic of overbank sedimentation in a distal floodplain environment (Selley, 1996; Miall, 2010). The presence of black carbonaceous matter in the massive mudrock deposits probably reflects moderate growth of vegetation on the floodplain where paleosols

developed (Kraus, 1997). The randomly dispersed carbonate nodules in the reddish white claystone and clayey siltstone beds probably characterize a floodplain environment (Kraus, 1997), and represent an initial stage of calcrete formation under seasonally arid to semi-arid climatic conditions (Huerta and Armenteros, 2005; Li et al., 2009; Tanner and Lacus, 2006). The vertically-oriented downward stripes and patches of reddish white, red and purple mottles in the claystone, clayey siltstone and mudrock are characteristic features of overbank (floodplain) deposits formed under low-energy conditions, low sedimentation rates and well-oxygenated environment in a drier climate and a highly variable water table (Kraus, 1997; Kraus and Gwinn, 1997; Retallack, 1997; Keighley, 2008; Li et al., 2009; Zhou et al., 2015). Low-angle cracks filled by reddish white clays in the mudrock seem to be vertic features (Tanner and Lacus, 2006), which indicate a seasonally aridity and less humidity (Tanner and Lacus 2006). Reddish coloration of mudstone suggests well-drained, oxidizing conditions of the floodplain, whereas grayish white and yellow coloration are produced in poorly drained, commonly waterlogged, distal floodplain conditions (Kraus and Gwinn, 1997; Retallack, 1997). The fining upward beds suggest that the alluvial system was fed by an ephemeral braided river (Miall, 1978, 2010; Selley, 1996).

4.2. Shallow lacustrine/palustrine facies association: FA-2

Description: FA-2 forms the upper part of the studied succession (Sn-2), and reaches up to 15 m in thickness (Figs. 2, 3). The rocks of this facies

association crop out as a cliff-forming unit (Fig. 4f). They show desiccation cracks and are pierced by root casts (Fig. 6d). They consist of an alternation of marlstone, mudrock, dolostone and dolomitic limestone. They are barren of marine fossils. Some *Charophytes* (Shamah and Helal, 1993) and small gastropod moulds were recognized (Fig. 6e). In addition, intercalation of gypsum layers (Fig. 6d) and stromatolitic dolostone beds (Fig. 6f) are found in this facies association. The marlstones and limestones are massive and yellowish white in color. The mudrock is dark to brownish grey and massive as well. Both dolostone and dolomitic limestone are grayish white to white, thin-bedded, pitted, concretionary in parts, and they form protruding ledges. Colour mottling is noticed in some dolostone beds. Microscopically, the dolostone displays two textural types: fine-crystalline, subhedral to euhedral dolomite rhombs (Fig. 7a, b) and micro-spherical (sub-rounded to rounded) dolomite crystals (Fig. 7c, d). All these dolomite crystals show similar size (less than 20 μm) and lack replacement textures. The limestone is mainly composed of micrite.

Interpretation: The carbonate rocks of FA-2 (micritic limestone, dolomicrite and marlstone) that are barren of marine fossils closely resemble deposits of short-lived shallow lakes or ponds with low-gradient margins (e.g., Platt and Wright, 1991; Abdul Aziz et al., 2003; Huerta and Armenteros, 2005; Alçiçek and Jiménez-Moreno, 2013). The small gastropod fossils and *Charophytes* indicate brackish shallow lake environments with water depth of lesser than 10 m (Sim et al., 2006). Occurrence of micritic limestones that lack any

sedimentary structures and without marine fossils are not unusual features of lake carbonates (Abdul Aziz et al., 2003; Huerta and Armenteros, 2005). The massive mudrock and marlstone separating carbonate beds can be attributed to lake flooding episodes, where the lake water becomes slightly brackish (Saez and Cabrera, 2002). In addition, gypsum layers and stromatolitic carbonate interbeds points to an evaporative environment under semi-arid climate during the final stage of lake development (Platt and Wright, 1991). The desiccation cracks, root traces and colour mottling in the carbonate rocks of the FA-2 provide evidence of subaerial exposure and paleopedogenic modifications in arid and semi-arid regions to form so-called palustrine carbonates (Platt and Wright, 1992; Alonso-Zarza, 2003; Huerta and Armenteros, 2005; Wanas and Soliman, 2014).

The fine-crystalline (< 20 μm), subhedral to euhedral rhombohedral dolomite crystals can be interpreted as early diagenetic in origin (Tucker, 2001), whereas micro-spherical (rounded to sub-rounded) dolomite crystals (micritic-size, < 20 μm) barren of marine fossils are similar to those formed as microbially-induced primary dolomite precipitates in shallow alkaline lakes (e.g., Vasconcelos and McKenzie, 1997; García del Cura et al., 2001; Calvo et al., 2003; Bréhéret et al., 2008; Huerto et al., 2010; Preto et al., 2015). The primary origin of the recognized micro-spherical dolomite can be indicated by petrographic features such as homogeneous size, finely-crystalline texture (micritic-size, < 20μm; Fig. 7c, d), and absence of replacive calcite (Last, 1990; García del Cura et al., 2001; Sáez and Cabrera, 2002; Wanas, 2002; Abdul Aziz

et al. 2003; Bréhéret et al., 2008). The occurrence of this micro-spheroidal dolomite provides evidence for semi-arid to arid climate (García del Cura et al., 2001, Wanas and Abu El-Hassan, 2006). In the light of the foregoing, it may be suggested that the rocks of FA-2 were deposited in a slightly brackish water shallow lacustrine environment under arid to semiarid climatic conditions. These shallow lacustrine deposits were also subjected to episodically subaerial exposure resulting palustrine carbonates.

5. Sequence stratigraphy

Sequence stratigraphy has been widely used for marine strata (Catuneanu, 2006), and has evolved towards the analysis of continental strata in different geological settings (e.g., Wright and Marriott, 1993; Shanley and McCabe, 1994; Van Wagoner, 1995; Aitken and Flint, 1995; Olsen et al., 1995; Carroll and Bohacs, 1999; Martinsen et al., 1999; Bohacs et al., 2000; Plint et al., 2001; Cleveland et al., 2007; Fanti and Catuneanu, 2010; Scherer et al., 2015). Martinsen et al. (1999) and Scherer et al. (2015) argued that alluvial-lacustrine depositional sequences are composed only of two systems tracts, formed as a result of changes in the balance between accommodation space (A) and sediment supply (S). The two systems tracts were named: Low- and High-accommodation Systems Tracts. The Low-accommodation Systems Tract (LAST) is characterized mainly by amalgamated alluvial channel deposits, in contrast to the High-accommodation Systems Tract (HAST) that is formed by single-storey, ribbon or sheet alluvial channel sand bodies

encased within fine-grained overbank deposits or lacustrine-dominated successions (Martinsen et al., 1999; Scherer et al., 2015). The HAST takes place where the A/S ratio close to or above 1 (i.e., sediment supply can not fill the available accommodation space and flooding occurs). On the other hand, the LAST occurs where the A/S ratio is between 0 and 1, but close to 0 (i.e., sediment supply fills the available accommodation space and some bypass may occur). Also, the sequence boundary occurs where the A/S ratio is negative (i.e., no accommodation space exists, which results in sediment bypass and erosion) (Martinsen et al., 1999; Scherer et al., 2015).

In this study, we highlight the sequence stratigraphic terminology of alluvial-lacustrine strata of Martinsen et al. (1999) and Scherer et al. (2015). Accordingly, a single depositional sequence, showing an overall fining-upward trend, from alluvial deposits passing upward to shallow lacustrine deposits, is determined (Figs. 2, 3). This sequence is bounded by two sequence boundaries (SB-1 and SB-2), and consists of two systems tracts (LAST and HAST) (Figs. 2, 3). The sequence boundaries are marked by disconformity surfaces at the base and top of the studied distal-alluvial and lacustrine successions. The basal Sequence Boundary (SB-1) is marked by subaerial deposits overlying erosively the Transgressive Systems Tract (TST) that represents the marine foraminiferal limestones of the lower unit of the Sannor Formation. The upper Sequence Boundary (SB-2) marks the abrupt facies change from shallow lacustrine deposits to marine foraminiferal limestones of the upper unit of the Sannor Formation (Figs. 2, 3). These

sequence boundaries were formed where no accommodation space exists, and there is subaerial exposure (i.e., A/S ratio was negative). Conglomerate (*Gcm, Gmm* and *Gh*) and pebbly sandstone deposits (*Sp, Sh, Sm*) in the lower part of the succession reflect a LAST, where there is an increase of ephemeral braided stream and sheet flood sediment supply relative to accommodation space (i.e., A/S ratio was between 0 and 1, but close to 0). On the other hand, the mudrock, silty claystone of distal floodplain facies (*Fsm; Fm*) and its overlying lacustrine facies (FA-2) correspond to a HAST (Fig. 3), where there is a decrease in fluvial discharge relative to accommodation space (i.e., A/S ratio close to or above 1).

6. Paleoclimatic conditions

In continental stratigraphic successions, paleoclimatic conditions can be inferred from the study of paleopedogenic features (e.g., Kraus, 1999; Wanas and Abu-El-Hassan, 2006; Srivastava et al., 2010; Meier et al., 2014), pollen assemblages (e.g., Zobaa et al., 2011; Alçiçek and Jiménez-Moreno, 2013; Watson and Dallwitz, 2015) and stable $\delta^{18}O$ and $\delta^{13}C$ isotopes (e.g., Alçiçek and Jiménez-Moreno, 2013; Li et al., 2013; Meier et al., 2014; Heilbronn et al., 2015). These properties are described from the middle unit of the Sannor Formation (Sn-2) as discussed below.

6.1. Paleopedogenesis (Paleosols)

A variety of macro- and microscopic paleopedogenic features are identified in both floodplain-dominated alluvial (FA-1) and shallow lacustrine

(FA-2) facies associations from the middle unit of the Sannor Formation. These features are described and interpreted below.

6. 1.1. Macroscopic features

Description: The macro-paleopedogenic features were observed in the mudrock and carbonate beds of the floodplain-dominated alluvial (FA-1) and shallow lacustrine deposits (FA-2). Most remarkable pedogenic feature comprise colour mottling (Figs. 4e, 5e, f; 6a, b), root traces (Figs. 5h, 6d), carbonaceous matter (Fig. 5h), carbonate nodules (Fig. 5g) and vertic features (Figs. 6c). In conglomerate and pebbly sandstone deposits of FA-1, no pedogenic features were noted.

Interpretation: Calcareous nodules in the mudrock of the FA-1 could represent initial stage of calcrete formation (calcisol) under arid to semi-arid climatic conditions (Mack et al., 1993; Tanner and Lacus, 2006; Li et al., 2009). The reddish white, red and purple mottles in the mudrocks of FA-1 mark development of oxisol (Mack et al., 1993; Kraus, 1999). They indicate well-drained floodplains in a drier climate (Bown and Kraus, 1987; Kraus, 1997; Kraus 1999; Cleveland et al., 2007; Retallack, 2008). They also suggest a variable water table that causes alternation of oxidizing and reducing conditions (Tanner and Lacus, 2006). The development of vertic features in the mudrock of FA-1 reflects pedogenesis (vertisol) (Mack et al., 2003), and indicates a seasonal aridity (Tanner and Lacus, 2006). The root traces, color mottling and desiccation cracks in the carbonate and mudrock deposits of the

FA-2 provide evidence of terrestrial conditions, soil development and episodic dry periods (Platt and Wright, 1991; Retallack, 1997; Alonso-Zarza, 2003).

6.1.2. Microscopic features

Description: The micro-pedogenic features in the floodplain deposits (FA-1) include illuviated and Fe and Mn oxides patches/micro-nodules. Clay illuviation is recognized by the high concentration of well-oriented clays that fill irregular fractures within the groundmass (Fig. 8a), and/or coat detrital grains (Fig. 8b). The illuviated clays are Mg-rich smectite showing curved plate's morphology (Fig. 8c). Fe and Mn oxides (and/or oxyhydroxides) occur as patches and micro-nodules (Fig. 8d). In the lacustrine carbonate deposits (FA-2), the microscopic pedogenic features include rootlets showing iron oxide mineralization (Fig. 8e), dense micritic mass with gradational boundaries with the surrounding groundmass (Fig. 8f), micro-spherical, micritic-sized, homogeneous dolomite crystals (Fig. 8g) and Fe-Mn oxides-micronodules (Fig. 8h).

Interpretation: Illuviated clays of Mg-smectite composition reflect pedogenesis under arid to semi-arid climatic condition (Buck et al., 2004; Srivastava et al., 2010; Gurel and Kadir, 2010). The formation of micritic-sized, homogeneous spheroidal dolomites can be related to pedogenic (soil) processes at the sediment–atmosphere interface in highly alkaline-Mg-rich-mediated lacustrine/alluvial fan lime-mudstones under relatively arid climates (García del Cura et al., 2001; Buck et al., 2004; Kearsey et al., 2012; Casado et al., 2014). The presence of root traces provides evidence for terrestrial

conditions and pedogenesis (Szrek et al., 2015). Patches and micro-nodules of Fe and Mn oxides (and/or oxyhydroxides) reflect fluctuations in redox potential associated with variable periodic water table (McCarthy et al., 1998; Tanner and Locus, 2006).

6.2. Pollen analysis

Description: Among the 5 samples analyzed for pollen analysis (EGH-6, 7, 8, 9, 11), sample number EGH-6 contained negligible organic matter content and only two pollen grains thought to be *Momipites* were found. This was anyway hard to confirm due to their orientation, faint colour, and inadequate preservation. The other 4 investigated samples (EGH-7, 8, 9, 11) contain fossil pollen grains that were classified as *Momipites coryloides*, *Triatriopollenites triangulus*, *Pinuspollenites* (Figs. 2, 9). These pollen grains are similar to those of the modern subfamily Chenopodioideae of the family Amaranthaceae. *Momipites coryloides* (Fig. 9). The total particulate organic matters (POM) components occur with different percentage (Fig. 10). Among the different POM components (see Tyson, 1993, 1995, for details) that can be found in sedimentary rocks, only opaque phytoclasts, degraded phytoclasts, and palynomorphs were recorded from the studied samples.

Interpretation: Low POM diversity can be attributed to provide oxidation in the depositional environment, which can be supported by the dominance of opaque phytoclasts. These are commonly derived from: a) the oxidation of woody fragments as a result of sediment reworking and/or long transport, b)

post depositional diagenesis and alteration, or c) natural wildfires (as charcoal) (Tyson, 1993; Zobaa et al., 2011). In the present study, the high percentage of opaque phytoclasts can be due to: 1) high energy oxic conditions during prolonged sediment transport, and 2) in-situ post depositional oxidation as a result of dry-out or low lake level, exposing bottom sediments to highly oxygenated conditions (Zobaa et al., 2011). The low POM diversity may also be alternatively interpreted as a part of organic poor facies accumulated in areas covered by sporadic vegetation, similar to present day arid/desert conditions.

Despite their scarcity and in absence of marine fossils, the recovered palynomorphs provide valuable information with regard to age dating and the prevailing floral cover. *Momipites coryloides* is thought to belong to the wind-pollinated trees of the *Engelhardia-Oromunnea-Alfaroa* complex of the angiosperm family Juglandaceae (Raymond et al., 1995; Jarzen et al., 2010). Pollen grains of *Pinuspollenites* are produced by the well-known conifer trees of the gymnosperm family Pinaceae. Such pine trees are evergreen, commonly high, with characteristic needle leaves. In contrast, pollen grains of the genus *Triatriopollenites triangulus* of the family Myricaceae and those of the family Amaranthaceae are usually produced by angiospermous small trees, herbs, and shrubs.

The aforementioned pollen association is neither diverse, nor abundant enough to make sound conclusions. However, the recovered flora represents a combined woodland–savanna ecosystem which had seasonally dry subtropical

to temperate climatic conditions (Watson and Dallwitz, 2015). The prevailing low moisture habitat may have prevented the woodland from completely developing and diversifying, providing a good opportunity for the herb/shrub community to spread. This scenario, combined with the previously suggested oxidizing conditions, explains well the complete absence of embryophytic spores in all of the analyzed samples.

6.3. Stable $\delta^{18}O$ and $\delta^{13}C$ isotopes

Stable $\delta^{18}O$ and $\delta^{13}C$ isotopes as a tool for interpreting paleohydrological and paleoclimatic conditions of lacustrine carbonates and alluvial carbonate nodules/concretions have been widely used (e.g., Talbot, 1990; Alonso-Zarza, 2003; Leng and Marshall, 2004; Alçiçek and Jiménez-Moreno, 2013; Li et al., 2013; Meier et al., 2014; Heilbronn et al. 2015). $\delta^{18}O$ and $\delta^{13}C$ values from selected samples of the Bartonian carbonate deposits are given in Table 2 and plotted in Figure 11. The data shows that the carbonate nodules in facies association-1 (FA-1) have negative $\delta^{18}O$ (-2.5 to -5.1‰) and $\delta^{13}C$ (-2.2 to -6.7 ‰) values. The carbonate deposits of facies association-2 (FA-2) display positive $\delta^{18}O$ values (1.5‰ to 2.9‰) and negative $\delta^{13}C$ values (-2.2‰ to -7.6‰). Three dolomicrite samples of the FA-2 show slightly positive $\delta^{18}O$ (-0.4 to 2.9‰) and $\delta^{13}C$ (1.3‰ to 0.3‰) values.

$\delta^{18}O$ and $\delta^{13}C$ of the carbonate nodules in FA-1: The negative $\delta^{13}C$ values (–6.4‰ to –6.7‰) combined with negative $\delta^{18}O$ values (–4.9‰ to –5.1‰) of the carbonate nodules in FA-1 suggest contribution of soil derived CO_2 and an influx of more diluted meteoric water to the alluvial floodplain deposits under

relatively arid to semi-arid climate (Eren, 2011; Kearsey et al., 2012; Li et al., 2013, 2014). Therefore, these carbonate nodules are very similar to the pedogenic carbonates.

$\delta^{18}O$ and $\delta^{13}C$ of the carbonate deposits in FA-2: The negative $\delta^{13}C$ values (−7.6‰ to −2.2‰) of the carbonate rocks of FA-2 indicate soil-derived CO_2 from root respiration under semi-arid climatic conditions (Li et al., 2013). This suggests that pedogenic modification and organic decay might have taken place (Eren, 2011; Li et al., 2013). The positive $\delta^{18}O$ (1.5‰ to 2.9‰) and $\delta^{13}C$ values (1.3‰ to 0.3‰) of the carbonate rocks of FA-2 indicate evaporative conditions under arid climate (Abdul Aziz et al., 2003; Eren, 2011; Alçiçek and Jiménez-Moreno, 2013). Therefore, the $\delta^{18}O$ and $\delta^{13}C$ values of carbonate deposits of FA-2 indicate that episodically arid-evaporative climates have often interrupted lake development during some time intervals throughout the Bartonian. The covariance between $\delta^{13}C$ and $\delta^{18}O$ can be used as a criterion to distinguish between closed and open lakes (e.g., Talbot, 1990; Li and Ku, 1997). It is also an index for paleoclimate (Talbot, 1990; Li et al., 2013). Consequently, the weak correlation (r= 0.056) between $\delta^{18}O$ and $\delta^{13}C$ values of the lacustrine carbonate sediments (FA-2) (Fig. 11) suggests a typical of primary carbonates formed in hydrologically open lakes that have short residence times (Talbot, 1990; Li et al., 2013). It also indicates arid to semi-arid climatic conditions. Such an overall semi-arid to arid climate is in accordance with that deduced by pollen assemblages and paleopedogenic features.

7. Controls on sedimentation

The stratigraphic architecture of alluvial-lacustrine successions can be controlled by three allogenic processes (relative sea level, climate, and tectonics), which in turn control accommodation space (Shanley and McCabe, 1994; Carroll and Bohacs, 1999; Bohacs et al., 2000; Pla-Pueyo et al., 2009; Huerta et al., 2011; Alonso-Zarza et al., 2012; Allen et al., 2013). The stratigraphic architecture of alluvial-lacustrine successions is influenced by relative sea level only in regions close to the coast (e.g., Schumm, 1993; Shanley and McCabe, 1994; Blum and Tornqvist, 2000; Amorosi and Colalongo, 2005). The recorded sedimentological data indicates that similar climatic conditions prevailed during the deposition of the studied succession. Thus, tectonic influence and sea-level change can be assumed to be the main controls of changes in sedimentation.

Although, the studied rocks were deposited in a continental context, without sedimentological and paleontological evidence of marine influence (see section 6), their underlying and overlying marine foraminiferal limestones (Fig. 2) may mark an influence of sea-level change in response with base-level fluctuation during the alluvial-lacustrine sedimentation. During sea-level lowstand, limited accommodation space and high alluvial activity occur, whereas in sea-level highstand the accommodation space increases in response to low alluvial activity (Holbrook et al., 2006). Consequently, the conglomerate and pebbly sandstone beds of braided

channel and sheet flood deposits of FA-1 can be deposited in response to period of low sea level. On the other hand, the mudstone deposits of the distal floodplain of FA-1 and its overlying shallow lacustrine deposits (FA-2) were deposited in response to period of high sea level.

Tectonic influence on deposition of the studied Bartonian deposits is evidenced by the abrupt contact between the alluvial and lacustrine sediments (Scherer et al., 2015) (Figs. 2, 3). This abrupt transition suggests major changes in the basin sedimentation regime and sediment supply from the source area, which is consistent with tectonically-driven alluvial-lacustrine successions (Plinth and Browne, 1994; Martinsen et al., 1999; Fanti and Catuneanu, 2010; Allen et al., 2013). Accordingly, tectonic movements controlled the A/S ratio during the accumulation of the alluvial-lacustrine succession (FA-1, FA-2). Tectonic uplift led to negative A/S ratio that is responsible for the generation of unconformities/sequence boundaries (SB). Sedimentation of gravel and sand deposits of the sheet-like channel fill of the lower part of FA-1 (LAST) corresponded to high alluvial activity, high sediment supply and low accommodation space (Huerta et al., 2011; Alonso-Zarza et al., 2012, Scherer et al., 2015). This could occur during episodic active tectonic movement that led to A/S ratio was between 0 and 1, sediment supply fills available accommodation space, allowing the accumulation of braided and sheet-like alluvial channel sands and gravels. As the low alluvial activity favors the formation of vertically stacked distal floodplain and lacustrine deposits (Alonso-Zarza et al., 2012). Accumulation of the upper

part of FA-1 (distal floodplain) and lacustrine deposits (HAST) took place during stages of low activity of the alluvial systems. This could develop during tectonic subsidence, where the rate of accommodation generation outpaces the rate of sediment supply (A/S ratio close to or above 1), thus favoring the development of both distal floodplain alluvial and lacustrine deposits (Alonso-Zarza et al., 2012; Scherer et al., 2015). Nevertheless, a syn-depositional fault system was not identified in the region (Haggag, 2010), which suggests that tectonics acted primarily through epeirogenic regional movements, which are capable of producing vertical movements on the basin margins, enlarging or reducing the amplitude of the resulting flexural deformation (Cloetingh and Kooi, 1992). This type of tectonic movement could be linked to a sag basin developed by reactivation of the Syrian-Arc during the Mid-Eocene (Said, 1990; Sallam et al., 2015).

8. Conclusions

The Mid-Eocene (Bartonian) continental sedimentary succession at Gebel El-Goza El-Hamra (NE Eastern Desert, Egypt) constitutes the middle unit (Sn-2) of the Sannor Formation. It is composed of siliciclastic rocks followed upward by carbonate beds. Two main facies associations were recognized: (1) floodplain-dominated alluvial facies association (FA-1), and (2) shallow lacustrine/palustrine facies association (FA-2). The FA-1 (up to 45 m thick) is composed mainly of carbonate nodules-bearing, mottled mudrock with subordinate sandstone and conglomerate deposits. This floodplain-

dominated alluvial facies association (FA-1) includes three lithofacies types: clast- and matrix-supported conglomerate (*Gcm; Gmm* and *Gh*), massive to planar cross-bedded sandstone (*Sm, Sh* and *Sp*), and mottled massive claystone–clayey siltstone-mudrock (*Fsm and Fm*) that were deposited in three alluvial sub-environments: ephemeral braided channel, sheet flood and distal floodplain, respectively. The FA-2 (up to 15 m thick) is made up of marlstone, micritic limestone and dolostone beds beds with *charophytes* and small gastropods. Pollen assemblages, stable $\delta^{18}O$ and $\delta^{13}C$ isotope values, and paleopedogenic features of the FA-1 and FA-2 reflect prevalence of arid to semi-arid climatic conditions during the Bartonian in the studied area.

In terms of sequence stratigraphy, the studied Mid-Eocene succession is made up of one depositional sequence bounded by two sequence boundaries (SB-1 and SB-2), and comprises low- and high- accommodation systems tracts (LAST and HAST). Facies architecture and stacking pattern of the depositional sequence reflect that the variation in the accommodation-to-sediment supply (A/S) ratio ratios was mainly controlled by sea-level change and local tectonic activity during reactivation of the Syrian Arc System.

Acknowledgments

We acknowledge the reviewers, Prof. J.P. Calvo; Prof. A.M. Alonso-Zarza (Facultad Ciencias Geologicas, Universidad Complutense de Madrid, Spain); Prof. L.H. Tanner (Geology Department, Le Moyne College, USA) and Prof. C. M. Scherer (Geociências, Instituto de Geociências, Brazil) whose suggestions and comments have improved the quality of the manuscript.

Special thanks extend to Prof. Jasper Knight (Editor in Chief, Sedimentary Geology) for help in the improvement of the manuscript and editorial support.

References

Abdul Aziz, H., Sanz-Rubio, E., Calvo, J.P., Hilgen, F.J., Krijgsman, W., 2003. Palaeoenvironmental reconstruction of a Middle Miocene alluvial fan to cyclic shallow lacustrine depositional system in the Calatayud Basin (NE Spain). Sedimentology 50, 211–236.

Abu El-Ghar, M.S., 2007. Eocene stratigraphy, facies, sequences and depositional history in Shabrawet area, North of Suez, Eastern Desert, Egypt. ISESCO 3, 23-42.

Aitken, J.F., Flint, S., 1995. The application of sequence stratigraphy to fluvial systems: an example from the Late Carboniferous of the Appalachians. Sedimentology 42, 3-30.

Al-Ahwani, M.M., 1982. Geological and sedimentological studies of Gebel Shabrawet area, Suez Canal District, Egypt. Annals Geological Survey of Egypt 12, 305-379.

Alçiçek, H., Jiménez-Moreno, G., 2013. Late Miocene to Plio- Pleistocene fluvio-lacustrine system in the Karacasu Basin (SW Anatolia, Turkey): Depositional, paleogeographic and paleoclimatic implications. Sedimentary Geology 291, 62–83.

Allen, J.P., Fielding, C.R., Rygel, M.C., Gibling, M.R., 2013. Deconvolving signals of tectonic and climatic controls from continental basins: an

example from the Late Paleozoic Cumberland Basin, Atlantic Canada. Journal of Sedimentary Research 83, 847-872.

Alonso-Zarza, A.M., 2003. Palaeoenvironmental significance of palustrine carbonates and calcretes in the geological record. Earth-Science Reviews 60, 261–298.

Alonso-Zarza , A.M., Meléndez, A., Martín-García, R., Herrero, M., Martín-Pérez, A., 2012. Discriminating between tectonism and climate signatures in palustrine deposits:Lessons from the Miocene of the Teruel Graben, NE Spain. Earth-Science Reviews 113, 41–160.

Alonso-Zarza, A.M., Zhao, Z., Song, C.H., Li, L.J., Zhang, J., Martín-Pérez, A., Martín-García, R., Wang, X., Zhang, Y., Zhang, M., 2009. Mudflat/distal fan and shallow lake sedimentation (upper Vallesian–Turolian) in theTianshui Basin, Central China: Evidence against the late Miocene eolian loess. Sedimentary Geology 222, 42-51.

Amorosi, A., Colalongo, M., 2005. The linkage between alluvial and coeval nearshore marine successions: evidence from the late Quaternary record of the Po River Plain, Italy. In: Blum, M., Marriott, S., Leclair, S. (Eds.), Fluvial Sedimentology VII. IAS Special Publication 35, pp. 257–275.

Blum, M., Tornqvist, T., 2000. Fluvial response to climate and sea-level change: a review and look forward. Sedimentology 47, 2–48.

Bohacs, K.M., Carroll, A.R., Neal, J.E., Mankiewicz, P.J., 2000. Lake-basin type, source potential, and hydrocarbon character: an integrated-

sequence-stratigraphic-geochemical framework. In: Gierlowski-Kordesch, E.H., Kelts, K.R. (Eds.), Lake Basins through Space and Time: AAPG Studies in Geology 46, pp. 3–34.

Bown, T.M., Kraus, M.J., 1987. Integration of channel and floodplain suites: I. Development sequence and lateral relations of alluvial paleosols. Journal of Sedimentary Petrology 57, 587-601.

Bréhéret, J.G., Fourmont, A., Macaire, J.J., Négrel, P., 2008. Microbially mediated carbonates in the Holocene deposits from Sarlième, a small ancient lake of the French Massif Central, testify to the evolution of a restricted environment. Sedimentology 55, 557–578.

Buck, B.J., Merkler, D., Mrozek, S., Harrison, B., Lato, L., 2004, Spheroidal Dolomite, Mg-Calcite, and Mg-Kutnohorite, Death Valley CA, USA: Implications for Genesis and Paleoenvironmental Interpretations, 12th International Meeting on Soil Micromorphology, Adana Turkey, pp. 1-2.

Calvo, J.P., McKenzie, J., Vasconcelos, C., 2003. Microbially mediated lacustrine dolomite formation: evidence and current research trends. In: Valero-Garcés, B.L. (Ed.), Limnogeology in Spain: A Tribute to Kerry Kelts. Consejo Superior de Investigaciones Cientificas, Madrid, pp. 229–251.

Carroll, A.R., Bohacs, K.M., 1999. Stratigraphic classification of ancient lakes: balancing tectonic and climatic controls. Geology 27, 99–102.

Casado, A.I., Alonso-Zarza, A.M., Iglesia, A.L., 2014. Morphology and origin of dolomite in paleosols and lacustrine sequences. Examples from the Miocene of the Madrid Basin. Sedimentary Geology 312, 50–62.

Catuneanu, O., 2006. Principles of Sequence Stratigraphy. Elsevier, New York, 386p.

Cleveland, D., Atchley, S., Nordt, L., 2007. Continental sequence stratigraphy of the Upper Triassic (Norian–Rhaetian) Chile strata, northern New Mexico, U.S.A.: allocyclic and autocyclic origins of paleosols-bearing alluvial successions. Journal of Sedimentary Research 77, 909–924.

Cloetingh, S., Kooi, H., 1992. Intraplate stresses and dynamical aspects of rifted basins. Tectonophysics 215, 167-185.

Eren, M., 2011. Stable isotope geochemistry of Quaternary calcretes in the Mersin area, southern Turkey – A comparison and implications for their origin. Chemie der Erde 71, 31–37.

Fanti, F., Catuneanu, O., 2010. Fluvial sequence stratigraphy: The Wapiti Formation, West-Central Alberta, Canada. Journal of Sedimentary Research 80, 320–338.

Fastovsky, D.E., McSweeney, K., 1987. Paleosols spanning the cretaceous-paleogene transition, eastern Montana and western north Dakota. Geological Society of America Bulletin 99, 66–77.

Fisher, J.A., Nichols, G.J., Waltham, D.A., 2007. Unconfined flow deposits in distal sectors of fluvial distributary systems: examples from the

Miocene Luna and Huesca Systems, northern Spain. Sedimentary Geology 195, 55–73.

García del Cura, M.A., Calvo, J.P., Ordóñez, S., Jones, B.F., Cañaveras, J.C., 2001. Petrographic and geochemical evidence for the formation of primary, bacterially induced lacustrine dolomite: La Roda 'white earth' (Pliocene, central Spain). Sedimentology 48, 897–915.

Gierlowski-Kordesch, E.H., 1998. Carbonate deposition in an ephemeral siliciclastic alluvial plain: Jurassic Shutte Meadow Formation, Hartford Basin, Newark Supergroup, USA. Palaeogeography, Palaeoclimatology, Palaeoecology 140, 161–184.

Gurel, A., Kadir, S., 2010. Palaeoenvironmental approach to the geology, mineralogy and geochemistry of an Early Miocene alluvial-fan to cyclic shallow-lacustrine depositional system in the Aktoprak Basin (central Anatolia), Turkey. Clay Minerals 45, 51-75.

Haggag, W., 2010. Structural setting an tectonic evolution of Gebel Shabrawet area and environs, North Eastern Desert, Egypt. Ph.D. Thesis, Faculty of Sciences, Benha University, 142pp.

Heilbronn, G., Boulvais, P., Marchand, E., Robin, C., Bourquin, S., Barrier, L., Jia, Y., Fu, B., Jolivet, M., 2015. Stable isotope characterization of pedogenic and lacustrine carbonates from the Chinese Tian Shan: Constraints on the Mesozoic–Lower Cenozoic palaeoenvironmental evolution. Chemie der Erde 75, 133-141.

Holbrook, J., Scott, R.W., Oboh-Ikuenobe, F.E., 2006. Base-level buffers and buttresses: a model for upstream versus downstream control on fluvial geometry and architecture within sequences. Journal of Sedimentary Research 76, 162–174.

Huerta, P., Armenteros, I., 2005. Calcrete and palustrine assemblages on a distal alluvial-floodplain: a response to local subsidence (Miocene of the Duero Basin, Spain). Sedimentary Geology 177, 235-270.

Huerta, P., Armenteros, I., Silva, P. G., 2011. Large-scale architecture in non-marine basins: the response to interplay between accommodation space and sediment supply. Sedimentology 58, 1716-1736.

Jarzen, D.M., Corbett, S.L., Manchester, S.R., 2010. Palynology and paleoecology of the Middle Miocene Alum Bluff flora, Liberty County, Florida, USA. Palynology 34, 261-286.

Kearsey, T., Twitchett, R.J., Newell, A.J., 2012. The origin and significance of pedogenic dolomite from the Upper Permian of the South Urals of Russia. Geological Magazine 149, 291–307.

Keighley, D., 2008. A lacustrine shoreface succession in the Albert Formation, Moncton Basin, New Brunswick. Canadian Petroleum Geologist Bulletin 56, 235–258.

Kraus, M.J., 1997. Lower Eocene alluvial paleosols: pedogenic development, stratigraphic relationships and paleosol/landscape associations. Palaeogeography, Palaeoclimatology, Palaeoecology 129, 387-406.

Kraus, M.J., 1999. Paleosols in clastic sedimentary rocks: their geologic applications. Earth-Science Reviews 47, 41-70.

Kraus, M.J., Gwinn, B., 1997. Facies and facies architecture of Paleogene floodplain deposits, Willwood Formation, Bighorn Basin, Wyoming, U.S.A. Sedimentary Geology 114, 33-54.

Last, W.M., 1990. Lacustrine dolomite: an overview of modern, Holocene and Pleistocene occurrences. Earth-Science Reviews 27, 221–263.

Leng, M.J., Marshall. G.D., 2004. Palaeoclimate interpretation of stable isotope data from lake sediment archives. Quaternary Science Reviews 23, 811–831.

Li, H.C., Ku, T.L., 1997. $\delta^{18}O$ - $\delta^{13}C$ covariance as a paleohydrological indicator for closed basin lakes. Palaeogeography, Palaeoclimatology, Palaeoecology 133, 69–80.

Li, X., Jenkyns, H. C., Zhang, C., Wang, Y., Liu, L., Cao, K., 2014. Carbon isotope signatures of pedogenic carbonates from SE China: rapid atmospheric *p*CO2 changes during middle–late Early Cretaceous time. Geological Magazine 151, 830-849.

Li, X., Sidun, C., Ke, C., Yunhua, C., Baoliang, X., Yannan, J., 2009. Paleosols of the Mid-Cretaceous: A Report from Zhejiang and Fujian, SE China. Earth Science Frontiers 16, 63-70.

Li, X., Xu, W., Liu, W., Zhou, Y., Wang, Y., Sun, Y., Liu, L., 2013. Climatic and environmental indications of carbon and oxygen isotopes from the Lower Cretaceous calcrete and lacustrine carbonates in Southeast and

Northwest China. Palaeogeography, Palaeoclimatology, Palaeoecology 385, 171–189.

Mack, G.H., James, W.C., and Monger, H. C., 1993, Classification of paleosols: Geological Society of America Bulletin 105, 129-136.

McCarthy, P.J., Plint, A.G., 1999. Floodplain paleosols of the Cenomanian Dunvegan Formation. Alberta and British Columbia, Canada: micromorphology, pedogenic processes and paleoenvironmental implication. In: Mariott, S.B., Alexander, J. (Eds.), Floodplain: Interdisciplinary Approaches. Geological Society London, Special Publication 163, pp. 289-310.

McCarthy, P.J., Martini, I.P., Leckie, D.A., 1998. Use of micromorphology for paleoenvironmental interpretation of complex alluvial paleosols: an example from the Mill Creek Formation (Albian), southwestern Canada. Palaeogeography, Palaeoclimatology, Palaeoecology 143, 87-110.

Miall, A.D., 1978. Lithofacies types and vertical profile models in braided river deposits, a summary. In: Miall, A.D. (Ed.) Fluvial Sedimentology. Canadian Society Petroleum Geologist Memoir 5, pp. 597–604.

Miall, A.D., 1996. The Geology of Fluvial Deposits. Springer-Verlag, Heidelberg, 582 pp.

Miall, A.D., 2010. Alluvial deposits. In: James, N.P., Dalrymple, R.W. (Eds.), Facies Models 4. Geological Association of Canada, St. John's Newfoundland, pp. 105–137.

Martinsen, O., Ryseth, A., Hansen, W.H., Fleshe, H., Torkildsen, G., Idil, S., 1999. Stratigraphic base level and fluvial architecture: Ercson Sandstonw (Campanian), Rock Springs Uplift, SW Wyoming, USA. Sedimentology 46, 235-259.

Meier, H.A., Driese, H.A., Nordt, L.C., Forman, S.L., Dworkin, S.I., 2014. Interpretation of Late Quaternary climate and landscape variability based upon buried soil macro- and micromorphology, geochemistry, and stable isotopes of soil organic matter, Owl Creek, central Texas, USA. Catena 114, 157-168.

Munsell Color, 2001. Munsell Rock Color Charts; Munsell Color: Baltimore, MD, USA.

Nemec, W., Steel, R.J., 1984. Alluvial and coastal conglomerates: their significant features and some comments on gravelly mass-flow deposits. In: Koster, E.H., Steel, R.J. (Eds.) Sedimentology of Gravels and Conglomerates. Canadian Society Petro1eum Geologist Memoir 10, pp. 1-31.

Oslen, T., Steel, R., Hogseth, K., Skar, T., Line Ros, S., 1995. Sequence architecture in a fluvial succession: Sequence stratigraphy in the Upper Cretaceous Mesaverde Group, Price Canyon, Utah. Journal of Sedimentary Research B65, 265-280.

Pla-Pueyo, S. Gierlowski-Kordesch, E.H., Viseras, C., Soria, J.M., 2009. Major controls on sedimentation during the evolution of a continental basin: Pliocene–Pleistocene of the Guadix Basin (Betic Cordillera, southern Spain). Sedimentary Geology 219, 97–114.

Platt, N.H., Wright, V.P., 1991. Lacustrine Carbonates: Facies Models, Facies Distributions and Hydrocarbon Aspects. In: Anadón, A., Cabrera, L., Kelts, K. (Eds.), Lacustrine Facies Analysis: International Association Sedimentologists Special Publication 13, pp. 57-74.

Platt, N.H., Wright, V.P., 1992. Palustrine carbonates at the Florida Everglades: towards an exposure index for the freshwater environment. Journal of Sedimentary Petrology 62, 1058-1071.

Plinth, A.G., Browne, G.H., 1994. Tectonic event stratigraphy in a fluvio-lacustrine, strike-slip setting: the Boss Point Formation (Westphalian A), Cumberland Basin, Maritime Canada. Journal of Sedimentary Research B64, 341-364.

Plint, A.G., McCarthy, P.J., Faccini, U.F., 2001. Nonmarine sequence stratigraphy: Updip expression of sequence boundaries and systems tracts in a high-resolution framework, Cenomanian Dunvegan Formation, Alberta foreland basin, Canada. American Association of Petroleum Geologist Bulletin 85, 1967–2001.

Preto, N., Breda, A., Dal Corso, J., Spotl, C., Zorzi, F., Frisia, S., 2015. Primary dolomite in the Late Triassic Travenanzes Formation,

Dolomites, Northern Italy: Facies control and possible bacterial influence. Sedimentology 62, 697–716.

Raymond, A., Phillips, M.K., Gennett, J.A., 1995. Palynology and paleoecology of lignites from the Manning Formation (Jackson Group) outcrop in the Lake Somerville Spillway. In: Warwick, P.D., Crowley, S.S. (Eds.), Coal Geology of the Paleocene-Eocene Calvert Bluff Formation (Wilcox Group) and the Eocene Manning Formation (Jackson Group) in east-central Texas. U.S. Geological Survey Open-File Report, pp. 95-595.

Retallack, G.J., 1997. Early forest soils and their role in Devonian global change. Science 276, 583-585.

Retallack, G.J., 2008. Soils of the Past; an Introduction to Paleopedology, Second Edition, Blackwell Science, Oxford, 404 pp.

Sáez, A., Cabrera, L., 2002. Sedimentological and palaeohydrological responses to tectonics and climate in a small, closed, lacustrine system: Oligocene As Pontes Basin (Spain). Sedimentology 49, 1073–1094.

Said, R., 1990. The Geology of Egypt. A.A. Balkema, Rotterdam, 734pp.

Sallam, E., Wanas, H.A., Osman, R., 2015. Stratigraphy, facies analysis and sequence stratigraphy of the Eocene succession in the Shabrawet area (north Eastern Desert, Egypt): An example for a tectonically-influenced inner ramp carbonate platform. Arabian Journal of Geosciences, DOI: 10.1007/s12517-015-1969-2

Sanz-Montero, E., Alonso-Zarza, A.M., Calvo, J.P., 1995. Carbonate pond deposits related to semi-arid alluvial systems: examples from the Tertiary Madrid Basin, Spain. Sedimentology 42, 437–452.

Scherer, M.S., Goldberg, K., Bardola, T. 2015. Facies architecture and sequence stratigraphy of an early post-rift fluvial succession, Aptian Barbalha Formation, Araripe Basin, northeastern Brazil. Sedimentary Geology 322, 43-62.

Schumm, S.A., 1993. River response to base-level changes: implications for sequence stratigraphy. Journal of Geology 101, 279–294.

Selim, S.S., El-Araby, A.A., Darwish, M., Abu Khadrah, A.M., 2012. Anatomy and development of tectonically-induced Middle Eocene clastic wedge on the Southern Tethys Shelf, North Eastern Desert, Egypt. GeoConvension, Vision, 1-6.

Selley, R.C., 1996. Ancient Sedimentary Environments and Their Subsurface Diagnosis. Chapman Hall, London, U.K., 300 pp.

Shamah, K., Helal, S., 1993. Stratigraphy of the Eocene sediments at Shabrawet area, Suez Canal environs, Egypt. Egyptian Journal of Geology 3, 275-298.

Shanley, K.W., McCabe, P.J., 1994. Perspective on the sequence stratigraphy of continental strata. American Association of Petroleum Geologists Bulletin 78, 544–568.

Sim, L.L., Chambers, J.M., Davis, J.A., 2006. Ecological regime shifts in salinised wetland systems. I. Salinity thresholds for the loss of submerged macrophytes. Hydrobiologia 573, 89-107.

Srivastava, P., Rajak, M.K., Sinha, R., Pal, D.K., Bhattacharyya, T., 2010.A high-resolution micromorphological record of the Late Quaternary paleosols from Gangae Yamuna interfluve: Stratigraphic and paleoclimatic implications. Quaternary International 227, 127-142.

Talbot, M.R., 1990. A review of the palaeohydrological interpretation of carbon and oxygen isotopic ratios in primary lacustrine carbonates. Chemical Geology 80, 261–279.

Tanner, L.H., Lacus, S.G., 2006. Calcareous paleosols of the Upper Triassic Chinle Group, Four Corners region, southwestern United States: Climatic implications. Geological Society of America, Special paper 416, pp. 53-74.

Tucker, M.E., 2001. Sedimentary Petrology: An Introduction to the Origin of Sedimentary Rocks. Blackwell Scientific Publications, Oxford, 260 pp.

Tyson, R.V., 1993. Palynofacies analysis. In: Jenkins, D.J. (Ed.), Applied Micropalaeontology. Kluwer Academic Publishers, Dordrecht, the Netherlands, pp. 153–191

Tyson, R.V., 1995. Sedimentary Organic Matter: Organic Facies and Palynofacies. Chapman and Hall, London, 615 pp.

Van Wagoner, J.C., 1995. Sequence stratigraphy and marine to nonmarine facies architecture of foreland basin strata, Book Cliffs, Utah, U.S.A. In: Van Wagoner, J.C., Bertram, G.T. (Eds.), Sequence Stratigraphy of Foreland Basin Deposits - Outcrop and Subsurface Examples from the Cretaceous of North America. American Association Petroleum Geologist Memoir 64, pp. 137-223.

Vasconcelos, C., McKenzie, J.A., 1997. Microbial mediation of modern dolomite precipitation and diagenesis under anoxic conditions (Lagoa Vermelha, Rio de Janerio, Brazil). Journal of Sedimentary Research 67, 378–390.

Wanas, H.A., 2002. Petrography, geochemistry and primary origin of spheroidal dolomite from the Upper Cretaceous/Lower Tertiary Maghra El-Bahari Formation at Gabal Ataqa, Northwest Gulf of Suez, Egypt. Sedimentary Geology 151, 211-224.

Wanas, H.A., Abu El-Hassan, M.M., 2006. Paleosols of the Upper Cretaceous – Lower Tertiary Maghra El-Bahari in the northeastern portion of the Eastern Desert, Egypt: Their recognition and geological significance. Sedimentary Geology 183, 243-259.

Wanas, H.A., Soliman, H.E., 2014. Calcretes and palustrine carbonates in the Oligo-Miocene clastic–carbonate unit of the Farafra Oasis, Western Desert, Egypt: Their origin and paleoenvironmental significance. Journal of African Earth Sciences 95, 145-154.

Watson, L., Dallwitz, M.J., 1992. The families of flowering plants: descriptions, illustrations, identification, and information retrieval. http://delta-intkey.com/angio/

Wright, V.P., Marriott, S.B., 1993. The sequence stratigraphy of fluvial depositional systems: the role of floodplain storage. Sedimentary Geology 86, 203-210.

Zhou, Y., Retallack, G.J., Huang, C., 2015. Early Eocene paleosol developed from basalt in southeastern Australia: implications for paleoclimate. Arabian Journal of Geosciences 8, 1281-1290.

Zobaa, M.K., Zavada, M.S., Whitelaw, M.J., Shunk, A.J., Oboh-Ikuenobe, F.E., 2011. Palynology and palynofacies analyses of the Gray Fossil Site, eastern Tennessee: their role in understanding the basin-fill history. Palaeogeography, Palaeoclimatology, Palaeoecology 308, 433-444.

Zobaa, M.K., El-Beialy, S.Y., El-Sheikh, H.A., El-Beshtawy, M,K., 2013. Jurassic–Cretaceous palynomorphs, palynofacies, and petroleum potential of the Sharib-1X and Ghoroud-1X wells, north Western Desert, Egypt. Journal of African Earth Sciences 78, 51-65.

Figure captions

Fig. 1. Geological map of the Shabrawet area, NE Eastern Desert, Egypt (modified after Al-Ahwani, 1982).

Fig. 2. Lithostratigraphic succession of the studied rocks. Sn-1, Sn-2 and Sn-3 refer to the lower, middle and upper units of the Sannor Formation, respectively. SB: sequence boundary, TST: transgressive systems tract, LAST: low accommodation systems tract, HAST: high accommodation systems tract.

Fig. 3. Profile of the studied succession. For symbols and abbreviations see Fig. 2.

Fig. 4. Field photographs showing: (**a)** isolated conical hills of the studied succession; (**b)** three informal units (Sn-1, Sn-2 and Sn-3) of the Sannor Formation; **(c)** three successive parts (1, 2 and 3) of the studied succession (Sn-2); (**d)** lower part of the of the studied succession consisting of pebbly sandstone and conglomerate interbeds (arrows) within mudrock; **(e)** middle part of the studied succession that is made up of white silty mudrock and siltstone with vertically-aligned purple, violet to red colour mottles (Fig. 2e).

Fig. 5. Field photographs from lower part of the studied succession (FA-1) showing (**a)** conglomerate lens (arrow) within yellow mudrock; (**b)** sheet-like bodies of conglomerate and pebbly sandstone; **(c)** scoured surface between conglomerate and desiccated mudrock; **(d**) clast imbrications in conglomerate Note, the inverse grading and non-erosional base of conglomerate; **(e)** small-scale planar cross-bedding in the yellow-coloured silty sandstones; **(f)** reddish

white vertically-aligned stripes of reddish white illuviated claystone within grayish yellow mudrock; **(g)** dispersed carbonate nodules (arrows) within mudrock**; (h)** black patches of carbonaceous? (organic) matter (arrows) in mudrock.

Fig. 6. Field photographs from middle part of the studied succession showing: (**a)** vertically-aligned violet mottles within white mudrock; **(b)** violet to red mottles in the form of patches within white mudrock; **(c)** low-angle cracks filled by reddish white illuviated clay (vertic features); **(d)** root traces (white arrow) and gypsum layers (black arrow) within carbonate rock; **(e)** small gastropod fossils (white arrow) in carbonate bed. Scale length is 10 cm**; (f)** stromatolitic-like structure of carbonate bed. Scale length is 15 cm.

Fig. 7. Photomicrographs showing: **(a)** fine-crystalline dolomite rhombs. Sample No. EGH-12; (**b)** SEM image of fine-crystalline dolomite rhombs (arrow). Sample No. EGH-12; **(c)** micro-spherical dolomite crystals. Sample No. Calc-1, EGH-19; **(d**) SEM image and electron microprobe of micro-spherical dolomite (arrow). Sample No. EGH-19.

Fig. 8. Photomicrographs showing representative micro-pedogenic features in the studied rocks: **(a)** illuviated clays within irregular fractures in the groundmass. Sample No. EGH-6; **(b)** illuviated clays coating detrital grains; Sample No. EGH-10; **(c)** SEM image of Mg-rich smectitic clays; Sample No.

EGH-10; (**d)** Fe and Mn-oxide black patches within mudrocks. Sample No. EGH-8; **(e)** rhizoliths traces showing iron oxide mineralization. Sample No. EGH-19; **(f)** densely packed micrite (arrows) in dolomite groundmass**.** Sample No. EGH-12; (**g)** spheroidal dolomites with dispersed quartz grains. Sample No. EGH-19; **(h)** Fe-Mn oxide micronodules (arrows) within dolomite groundmass**.** Sample No. EGH-22.

Fig. 9. Plane-polarized photomicrographs showing: **(a)** general view of opaque phytoclast in the studied samples. Sample No. EGH-7, 5X; **(b**) degraded phytoclast particle. Sample No. EGH-7, 10X; **(c)** well preserved phytoclast particle. Sample No EGH-9, 20X; **(d)** dendritic-shaped phytoclast?. Sample No. EGH-11, 40X; **(e)** dark brown phytoclast particle which has almost become opaque. Sample No. EGH-8, 20X; **(f)** *Momipites coryloides* Wodehouse, 1933. Sample No. EGH-7, 40X; **(g)** probable grain of *Momipites coryloides*. Sample No. EGH-8, 40X; **(h)** *Triatriopollenites triangulus* Frederiksen, 1979. Sample No. EGH-8, 40X; **(i)** *Pinuspollenites* sp. Sample EHG-8, 40X; **(j)** fungal spore. Sample No. EGH-7, 40X.

Fig. 10. Percentage distribution of the major POM in the palynologically studied samples.

Fig. 11. $\delta^{18}O$ and $\delta^{13}C$ plots for carbonate samples of the FA-1 and FA-2.

Table 1. Summary of the identified lithofacies and their related environments**.**

Table 2. $\delta^{18}O$ and $\delta^{13}C$ values (VPDB‰) for carbonate samples taken from FA-1 and FA-2 of the studied succession. Calc = Carbonate nodules samples of the FA-1; EGH = Carbonate samples of the FA-2.

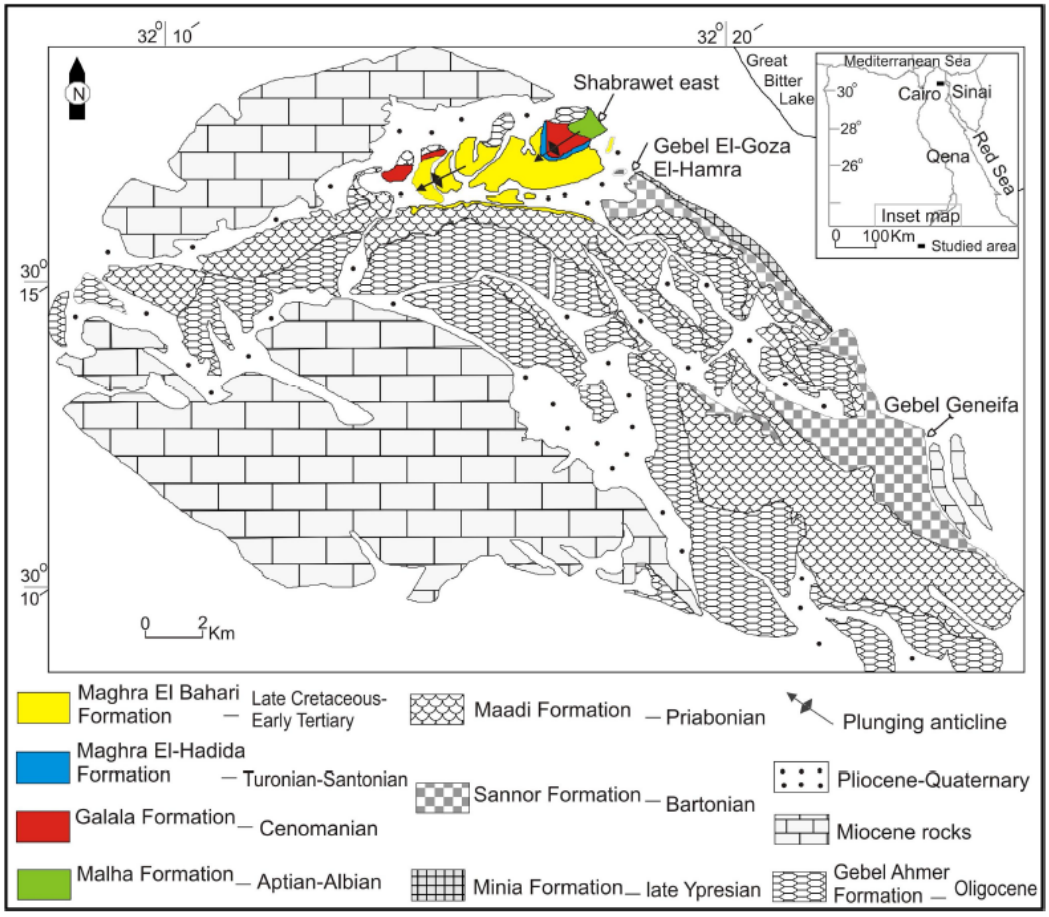

Figure 1

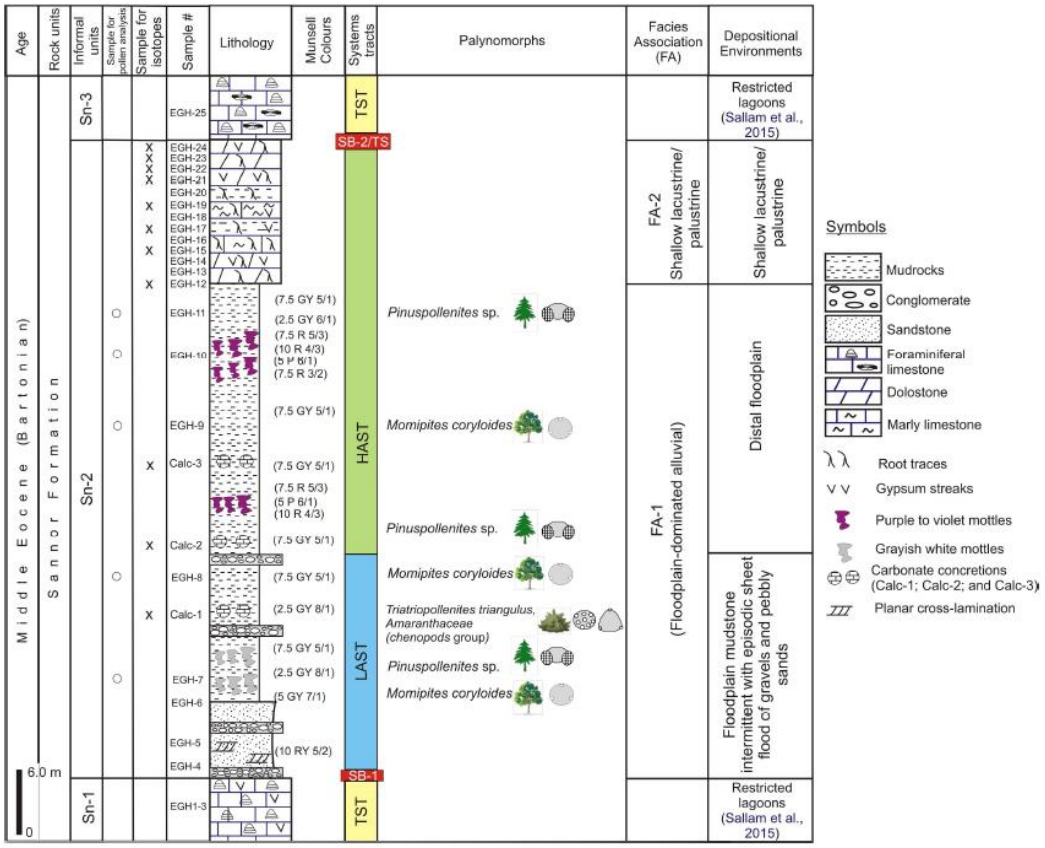

Figure 2

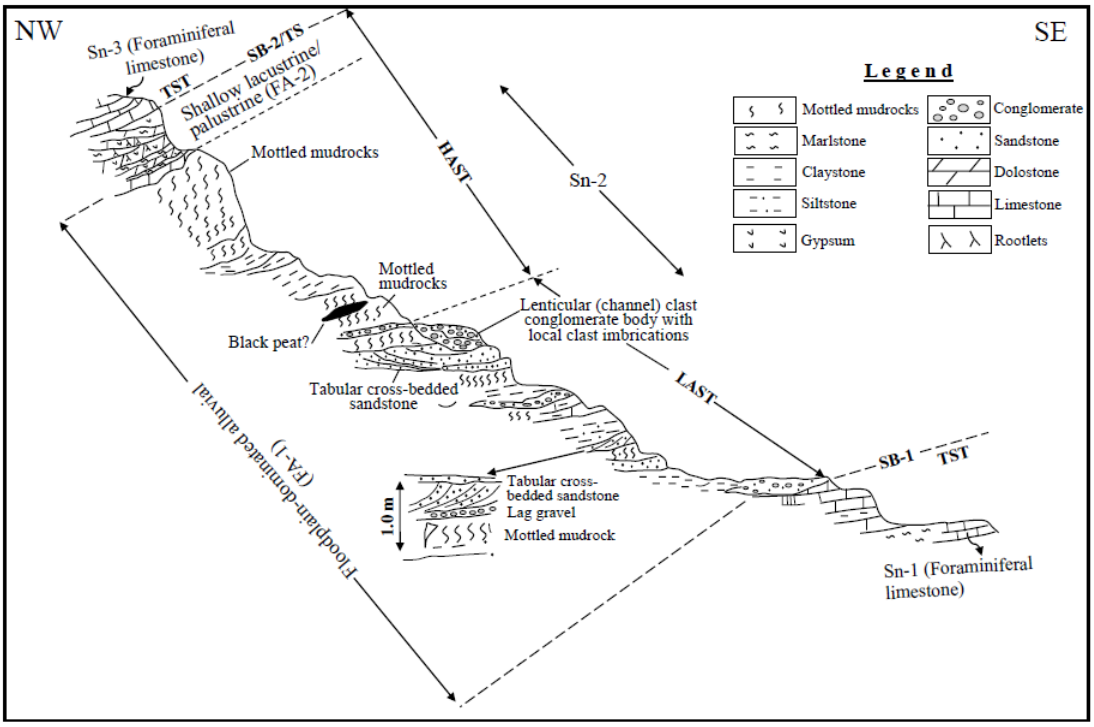

Figure 3

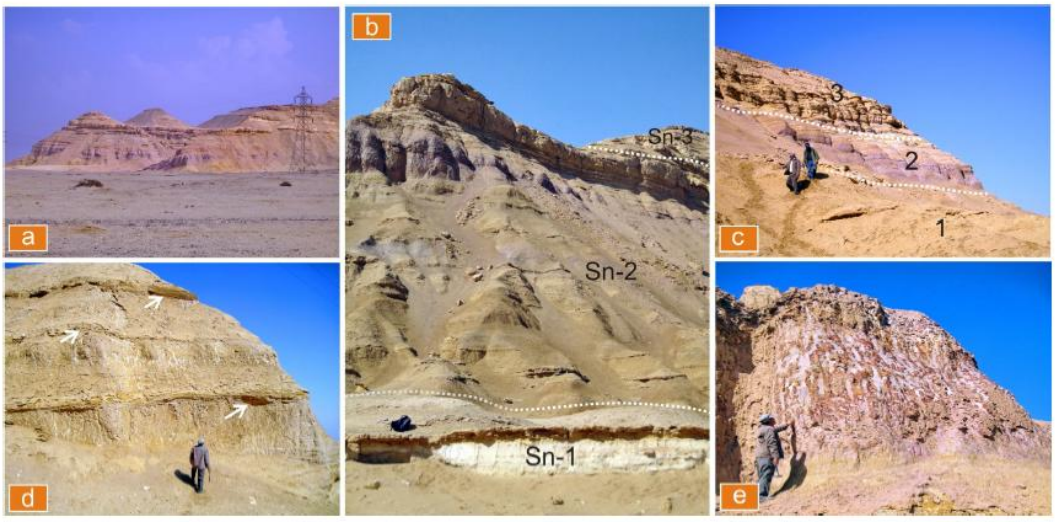

Figure 4

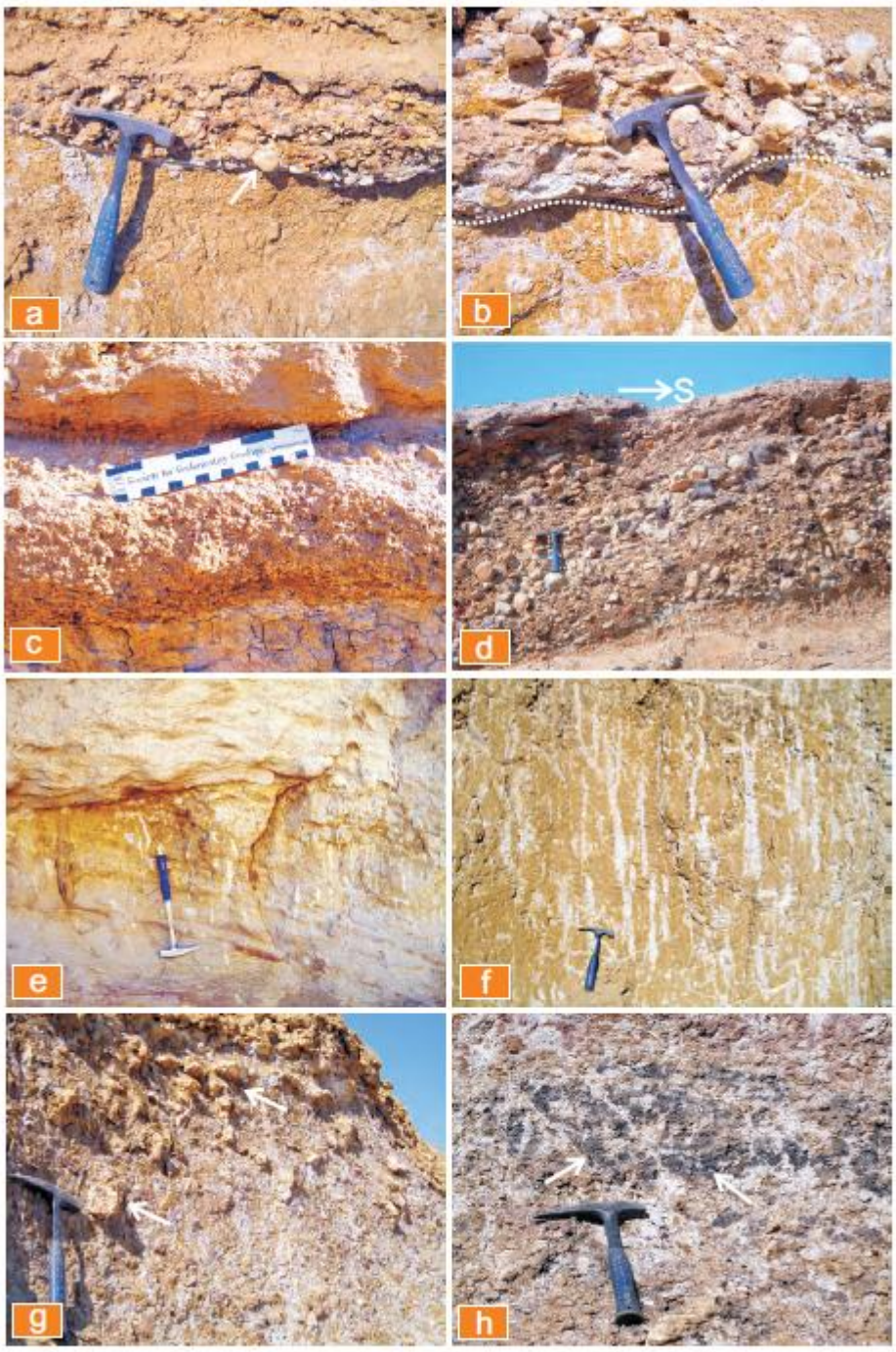

Figure 5

Figure 6

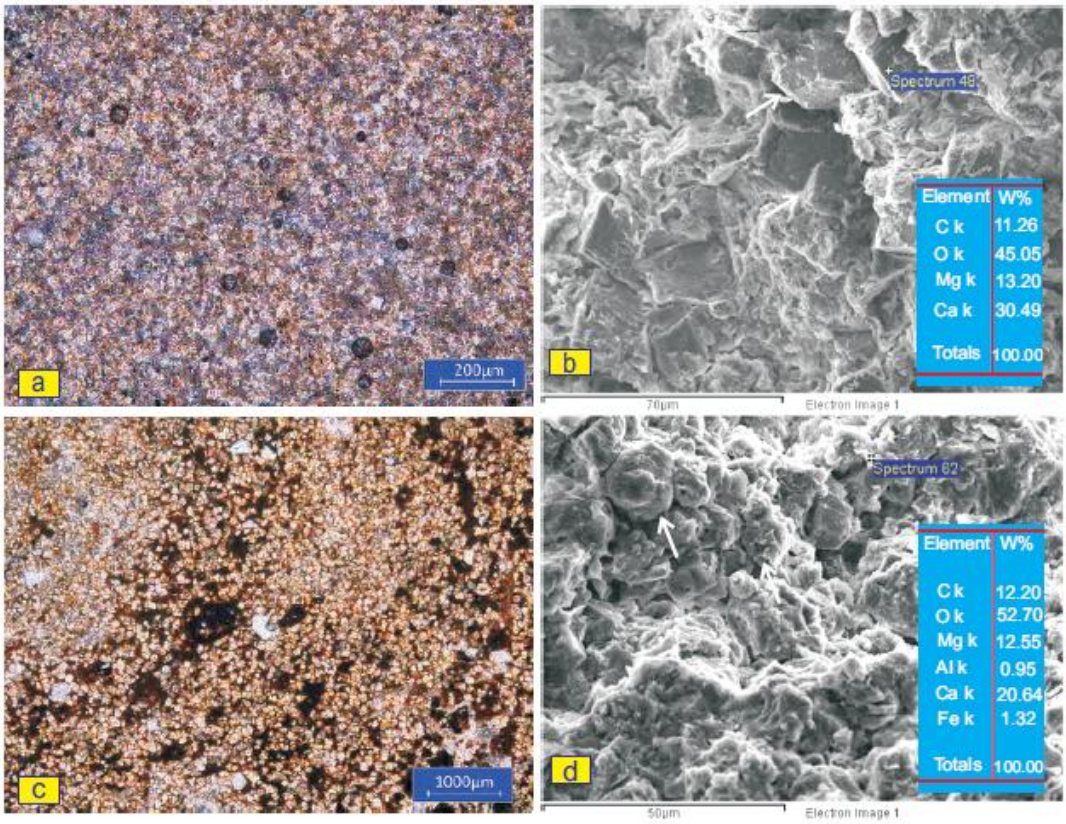

Figure 7

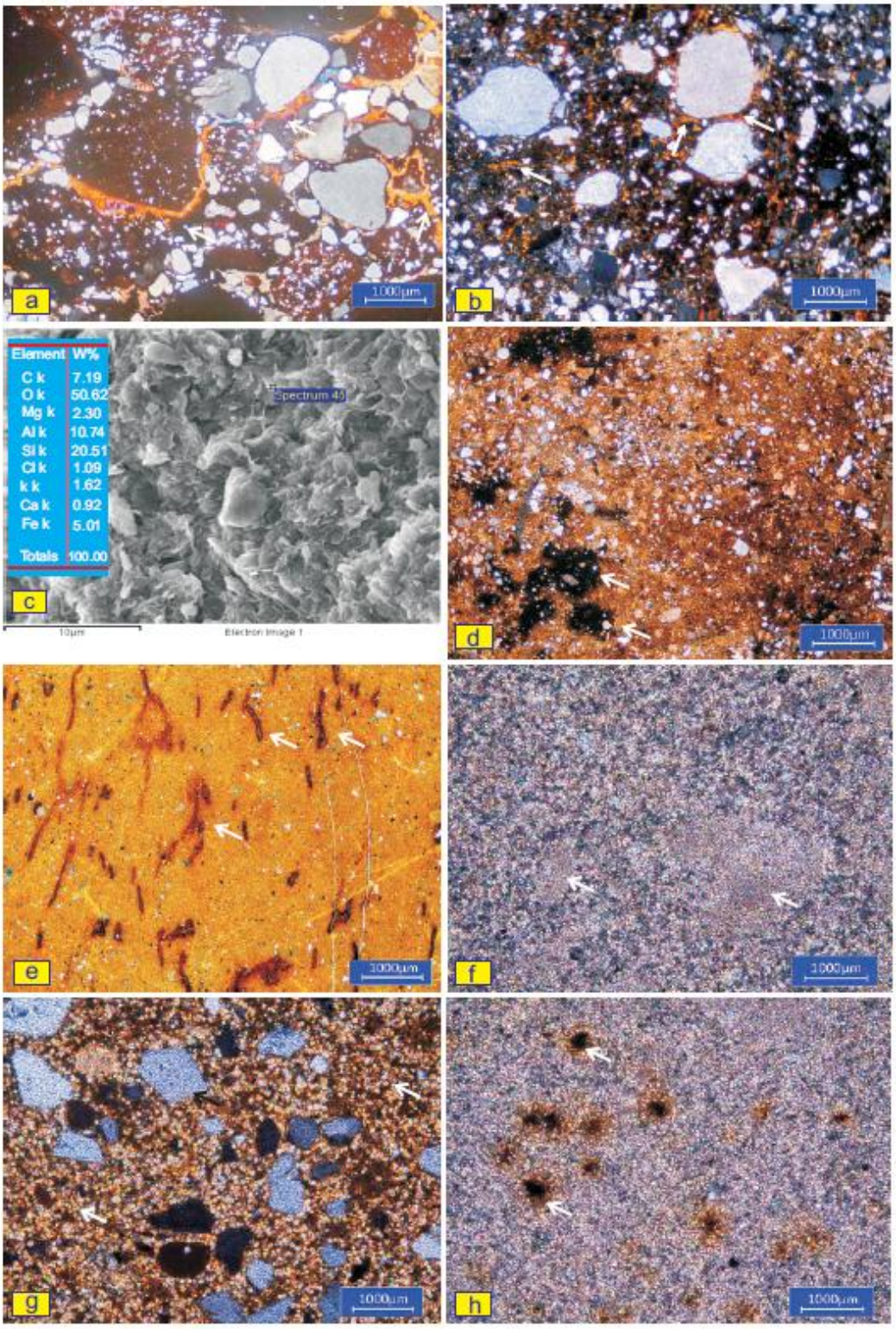

Figure 8

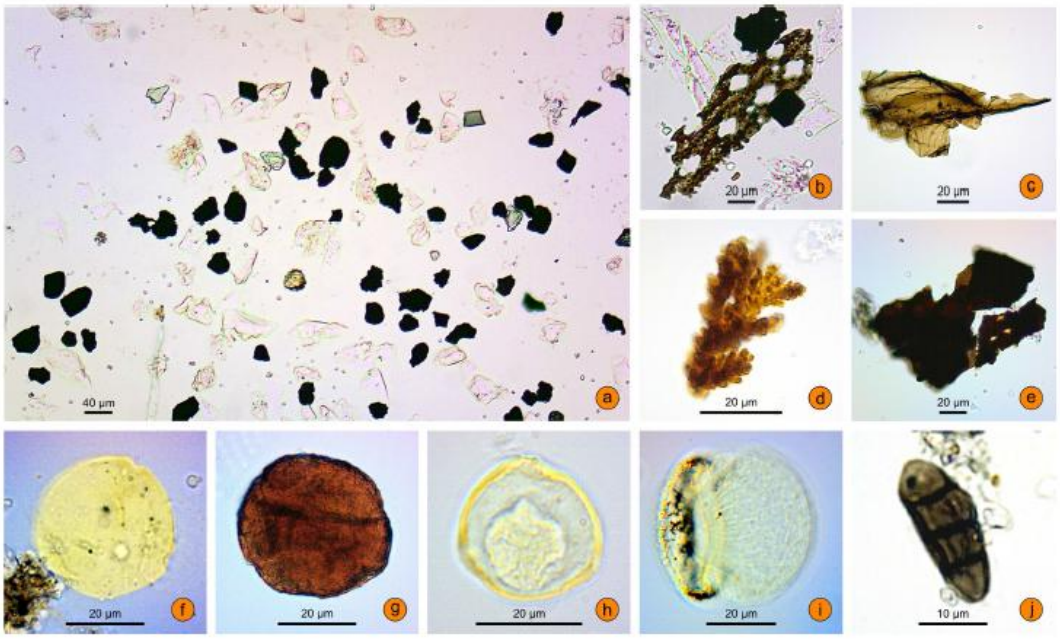

Figure 9

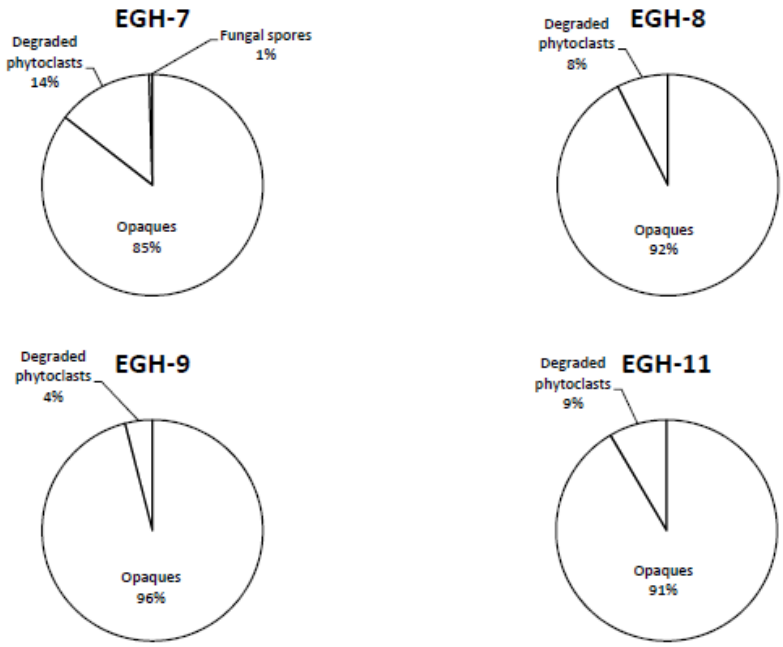

Figure 10

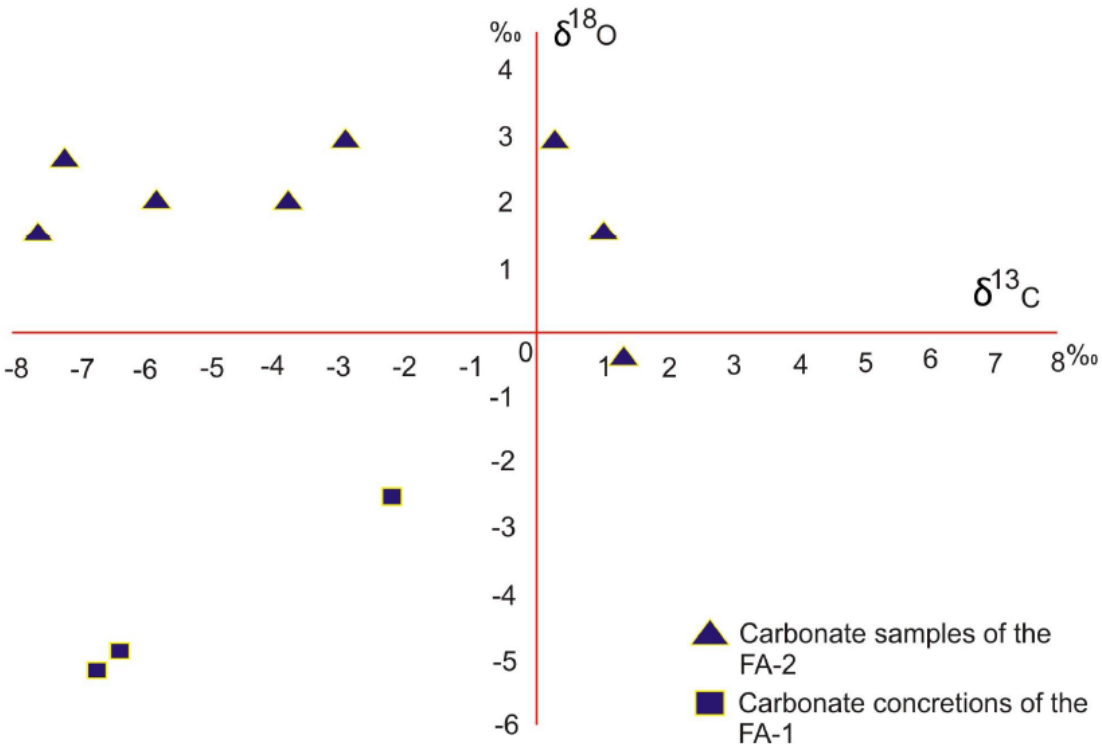

Figure 11

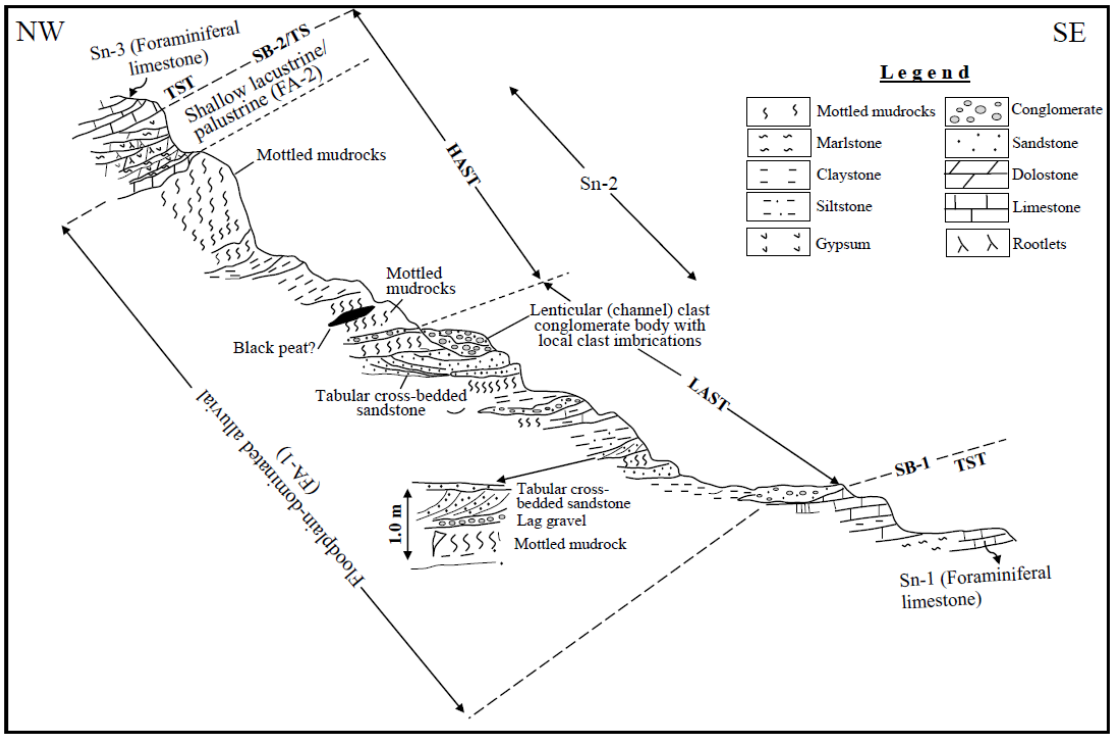

Graphical abstract

Highlights

The studied deposits were accumulated in floodplain-dominated alluvial and shallow lacustrine system. They show evidence of macro- and micro-pedogenicfeatures. They consist of low- and high-accommodation systems tracts. Arid to semiarid climate was prevailed in the studied area during Bartonian age.

Table 1

Facies association	Lithofacies types based on Miall (1978; 2010)	Description	Sedimentary structures	Interpretation
Shallow lacustrine/ palustrine (FA-2)		Intercalated dolomicrite, marlstone and mudrock beds. Small gastropods are noted	Thin-bedding; root traces; stromatolitic; nodular	Shallow lacustrine/palustrine (Alcicek and Jimenez, 2013); Wanas and Soliman, 2014)
Floodplain-dominated alluvial (FA-1)	Fm	Mudrocks; yellow in colour and include reddish white mottles and carbonate nodules	Vertic features	Overbank sedimentation; (Selley, 1996; Kraus, 1997; Miall, 2010)
	Fsm	Claystone and clayey siltstone; displaying red, violet and purple colour mottling	Massive	Distal floodplain deposits; (Selley, 1996; Miall, 2010)
	Sp	Sandstone; fine- to medium-grained; light grey to grayish yellow; moderately-sorted	Planar cross-bedding	Transverse bedforms (sand bars); upper flow regime (Miall, 1996; 2010)
	Sh	Sandstone; fine- to medium-grained; grey to faint yellow; pebbly; moderately-sorted	Horizontal lamination	Sheet flooding; upper flow regime (Kraus and Gwinn, 1997; Fisher et al., 2007)
	Sm	Sandstone; fine- to medium-grained; grey to faint yellow; pebbly; moderately-sorted	Sheet-like; massive	Sheet flood; braided fluvial channels (Alcicek and Jimenez-Moreno, 2013)
	Gh	Clast-supported conglomerate; the clasts are typically pebbly-sized; moderately-sorted; rounded to sub-rounded; discoidal-shaped	Local imbrication	Lag deposits; braided channel fills (Miall, 2010)
	Gmm	Matrix-supported conglomerate; the clasts are pebbly-sized up to cobble size; poorly-sorted; rounded to sub-rounded. The matrix is argillitic	Massive; inverse grading	Plastic debris flow (viscous) (Nemec and Steel, 1984; Miall, 2010)
	Gcm	Clast-supported conglomerate; the clasts are typically pebbly-sized; poorly-sorted; rounded to well rounded; elongated and discoidal-shaped	Massive	Braided channel fills with turbulent flow (Miall, 1978)

Table 2

Facies association	Sample No.	$\delta^{13}C_{VPDB‰}$	$\delta^{18}O_{VPDB‰}$
FA-2	EGH24	1.0	1.5
	EGH23	0.3	2.9
	EGH22	1.3	-0.4
	EGH21	-2.9	2.9
	EGH19	-3.8	2.0
	EGH17	-7.6	1.5
	EGH15	-5.8	2.0
	EGH12	-7.2	2.6
FA-1	Calc-3	-2.2	-2.5
	Calc-2	-6.7	-5.1
	Calc-1	-6.4	-4.9